ACS EARTH AND SPACE CHEMISTRY

http://pubs.acs.org/journal/aesccq

Article

Chirped-Pulse Fourier Transform Millimeter-Wave Spectroscopy of Furan, Isotopologues, and Vibrational Excited States

Timothy J. Barnum,* Kin Long Kelvin Lee, and Brett A. McGuire*

Cite This: *ACS Earth Space Chem.* 2021, 5, 2986−2994

Read Online

ACCESS | Metrics & More | Article Recommendations | Supporting Information

ABSTRACT: Recent astronomical detections of several five- and six-membered carbon rings in the interstellar medium (ISM) have expanded our understanding of the chemistry operative in diverse astrophysical environments. These discoveries prompt new interest in astronomical searches for the more chemically complex heterocycles, and laboratory studies of the rotational spectra of such molecules are a crucial first step. We present a new investigation of the rotational spectrum of the aromatic heterocycle furan (C_4H_4O) in selected bands from 75 to 295 GHz by chirped-pulse Fourier transform millimeter-wave spectroscopy. The improved determination of molecular constants is suitable for computing rest frequencies for astronomical searches throughout the millimeter-wave region. We also present new rotational analyses of the two singly substituted carbon-13 isotopomers and the two lowest vibrational excited states, ν_{11} and ν_{14}. Using the second data release from the GOTHAM spectral line survey of the starless cold core Taurus Molecular Cloud 1, we determine a new upper limit on the abundance of furan in this source, further demonstrating the peculiarly low abundance of heterocycles relative to pure hydrocarbon cycles in the ISM.

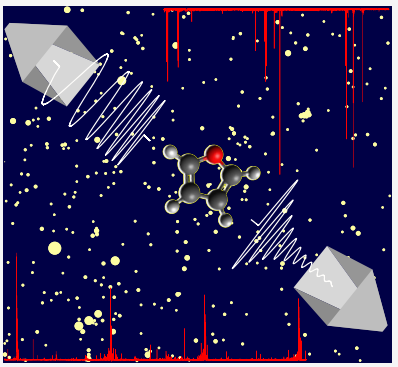

KEYWORDS: *rotational spectroscopy, millimeter wave, furan, heterocycle, TMC-1, astrochemistry*

Downloaded via MASSACHUSETTS INST OF TECHNOLOGY on January 20, 2022 at 14:37:27 (UTC).
See https://pubs.acs.org/sharingguidelines for options on how to legitimately share published articles.

1. INTRODUCTION

Despite their significance to terrestrial chemistry, five- and six-membered aromatic rings have only recently been identified in the interstellar medium (ISM).[1] Following the observation of benzonitrile (c-C_6H_5CN) in the quiescent molecular cloud Taurus Molecular Cloud 1 (TMC-1),[2] both five-membered[3,4] and bicyclic[5,6] species have been detected in this source in rapid succession. Benzonitrile has also recently been observed in four additional molecular clouds in different stages of prestellar evolution,[7] suggesting a ubiquitous aromatic chemistry operative in interstellar environments.

With these detections now secure and at remarkably high abundance, heterocyclic molecules, in which one or more carbon atoms has been substituted by a heteroatom, like N, O, or S, are the next logical step in chemical complexity to explore. Heterocycles play an essential role in biological chemistry, from the sugars and nucleobases that compose RNA to common motifs in pharmaceutical compounds.[8] While both N- and O-heterocycles have been identified in carbonaceous chondrites,[9,10] only a handful of rings have been unambiguously identified in the ISM at all, of which none are aromatic heterocycles.[11] In particular, searches for furan (C_4H_4O) and related five-membered heterocycles pyrrole (C_4H_5N) and imidazole ($C_3H_4N_2$) toward several sources have thus far been unsuccessful.[12−15]

The most recent search[14] established an upper limit abundance of furan in TMC-1 substantially higher than the derived abundances for recently detected aromatic species in this source.[2,5,6] Thus, more detailed or sensitive searches for these species are needed to constrain their abundance relative to the all-carbon rings. As demonstrated by the recent detections in TMC-1, such searches require high-precision laboratory data covering the regions of the strongest transitions at local excitation temperatures of 5−10 K.[5,16] For many small heterocycles, the Boltzmann distribution results in bright lines up through the 3 mm window, where laboratory data has often not yet reached.

Motivated by the significance of aromatic heterocycles to prebiotic chemistry and the rapid expansion of the aromatic chemical inventory of interstellar sources, we have revisited the rotational spectroscopy of furan in the millimeter-wave (mmW) region. We employed two chirped-pulse Fourier transform (CP-FT) mmW spectrometers to identify more than 200 new transitions in the frequency ranges from 75.6 to 99.6 GHz and from 260 to 295 GHz. In combination with previous microwave data, our new analysis has obtained a full set of quartic centrifugal distortion constants and four sextic constants. In addition, we identifed transitions belonging to both carbon-13 isotopomers in natural abundance and to two

Special Issue: Chemical Complexity in Planetary Systems

Received: June 2, 2021
Revised: August 20, 2021
Accepted: October 5, 2021
Published: October 20, 2021

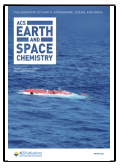

© 2021 American Chemical Society

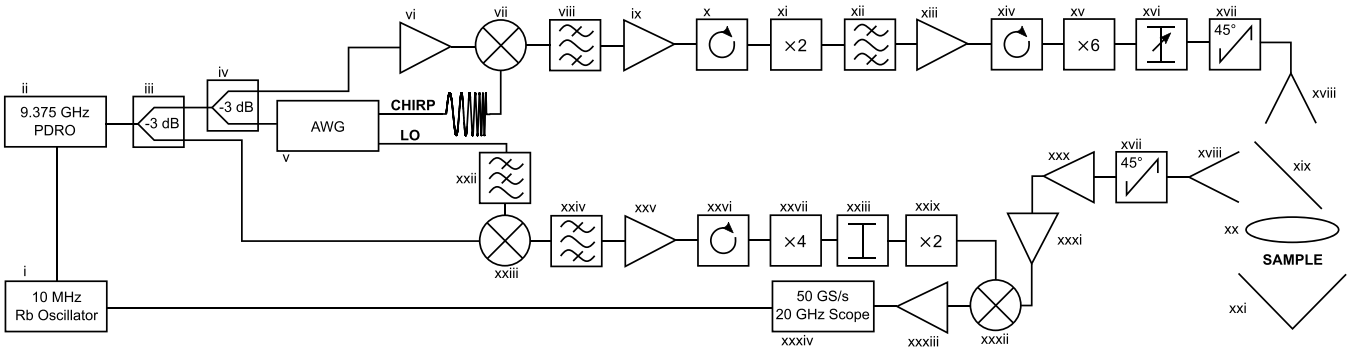

Figure 1. Schematic diagram of the W-band 75.6−99.6 GHz spectrometer. A stable dielectric resonator oscillator (PDRO, ii) operating at 9.375 GHz is phase-locked to a 10 MHz Rb frequency standard (i). The output of this oscillator is power-divided several times, and a portion serves as the sampling clock for the AWG (v). A chirped pulse is produced on channel 1 and upconverted by mixing with the fixed 9.375 GHz output of the PDRO. A bandpass filter selects only the lower sideband, which is subsequently multiplied by a factor of 12 and amplified to produce the W-band chirped pulse. Several bandpass filter and isolator stages serve to reduce spurious frequency content in the final excitation pulse. The chirp is broadcast from a rectangular standard gain horn and polarizes a molecular sample as described in the text. The molecular FID is detected at a second horn antenna and amplified by a low-noise amplifier (xxx) and power amplifier (xxxi) operating in the W band. This signal is then downconverted in a harmonic mixer (xxxii), before further amplification (xxxiii) and digitization on a high-speed oscilloscope (xxxiv). The local oscillator for the downconversion stage is generated by mixing the single-frequency output on channel 2 of the AWG with the 9.375 GHz PDRO. The upper sideband is selected, then amplified, and multiplied by a factor of 8 to generate the LO signal in the W band. A complete part list for this spectrometer may be found in the Supporting Information.

low-lying vibrational excited states of furan and observed and characterized perturbations in the vibrationally excited spectra. Throughout this work, we use the symmetry labels and vibrational mode ordering of Mellouki et al.[17] Finally, we searched for furan toward the quiescent molecular cloud TMC-1 and obtained a new upper limit on the column density of furan in this source.

2. EXPERIMENTAL AND COMPUTATIONAL METHODS

Rotational spectra of furan were collected in two instrumental setups by CP-FT mmW spectroscopy: a jet-cooled coaxial mmW spectrometer operating in the W band from 75.6 to 99.6 GHz and a room-temperature waveguide cell spectrometer operating between 260 and 295 GHz. To assist in the assignment of all spectra, quantum chemical calculations, including cubic force fields, were performed.

2.1. W-Band Chirped-Pulse Millimeter-Wave Spectroscopy. The 75.6−99.6 GHz spectrometer, shown schematically in Figure 1, is based substantially on the original design of Park et al.[18] Our design accomplishes the high phase stability required in the mmW spectral region by the use of a single-frequency source: a phase-locked dielectric resonator oscillator (PDRO, Miteq DLCRO-010-09375-3-15P) operating at 9.375 GHz, phase-locked to a 10 MHz Rb frequency standard (Stanford Research Systems FS725). A portion of the PDRO output is fed directly into an arbitrary waveform generator (AWG, Agilent Technologies M8190A) to serve as the sampling clock. Channel 1 of the AWG produces a chirped excitation pulse between 1 and 3 GHz, which is subsequently mixed with the 9.375 GHz PDRO and amplified and multiplied by a total factor of 12 to produce a chirped pulse in the W band. Bandpass filters after each frequency conversion step serve to reduce the spurious frequency content. The chirped excitation pulse is broadcast via a rectangular standard gain horn and passes through a wire-grid polarizer oriented to pass the linearly polarized radiation. The excitation pulse is then collimated by a polytetrafluoroethylene (PTFE) lens and enters the vacuum chamber, where it interacts with the molecular beam propagating coaxially with the radiation. Both excitation pulse and molecular free induction decay (FID) are reflected off of an aluminum roof-top reflector, oriented 45° relative to the polarization direction of the radiation, which produces a 90° rotation of the linear polarization. A second pass of the molecular sample occurs before radiation exits the vacuum chamber, now reflected by the wire-grid polarizer and focused by the PTFE lens onto a second rectangular standard gain horn. As a result of the low total power available in the mmW region, no protective switch is required to block the receiver unit from the excitation pulse. The molecular FID signal is amplified by a low-noise amplifier (Millitech LNA-10-02150) and an additional power amplifier (JPL Custom Unit) before entering a fundamental mixer (Millitech MXP-10-RFSSL). The LO signal fed to the mixer is a constant frequency produced by the second channel of the AWG, which is mixed with the same 9.375 GHz PDRO signal and multiplied by a total factor of 8 to reach the W band. The downconverted FID passes through an additional low-noise amplifier (Miteq AMF-7D-00101800-24-10P) and is then directly digitized on a fast oscilloscope (Tektronix DPO72004, 50 GS/s, 20 GHz). The Rb frequency standard provides a 10 MHz reference clock for the oscilloscope, and at least 1 million FIDs can be coherently averaged. To unambiguously assign transitions, the 24 GHz bandwidth was collected in two acquisitions with single sideband detection. A section of the W-band spectrum of furan appears in Figure 2.

The experimental chamber for the jet-cooled spectroscopy is a large six-way cross (MDC 1200-6) evacuated by a 10 in. water-cooled diffusion pump (Varian VHS-10). Furan, seeded at 5% in argon or helium at a stagnation pressure of 30 psi, was introduced through a pulsed supersonic expansion (General Valve Series 9 nozzle, 0.5 mm orifice). The nozzle was mounted directly behind the rooftop reflector, and the jet expansion passed through a small hole drilled in the center of the reflector. The observed rotational temperature of furan in this expansion was ∼5 K. The narrow velocity distribution in the propagation direction of the beam resulted in Doppler-broadened line widths of ∼75 kHz at 90 GHz, approximately 5

https://doi.org/10.1021/acsearthspacechem.1c00182
ACS Earth Space Chem. 2021, 5, 2986−2994

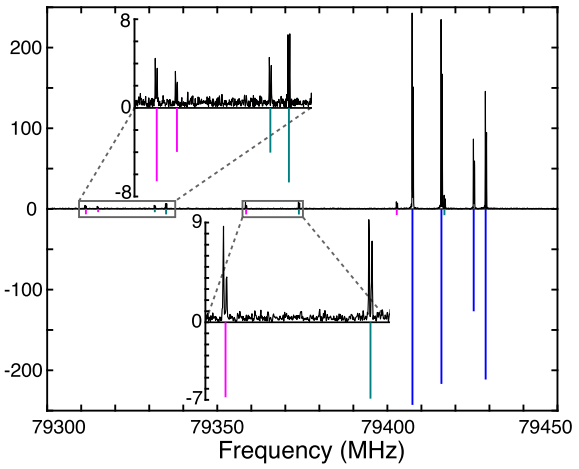

Figure 2. Section of the jet-cooled spectrum of furan collected with the W-band spectrometer. Doppler doublets as a result of the coaxial propagation of the molecular beam and millimeter-wave radiation appear for each transition. Simulated spectra of the ground state (blue), ν_{11} (teal), and ν_{14} (magenta) for the main isotopologue appear below the experimental spectrum, using the constants from Tables 1 and 4. The highlighted areas show the characteristic intensity patterns as a result of nuclear spin statistical weights for ν_{11} (a_2) and ν_{14} (b_1).

times narrower than observed in a transverse geometry.[18] The coaxial geometry produces Doppler doublets for every molecular signal, and the rest frequency was determined by the mean of the fitted line centers of the two Doppler components.

2.2. Waveguide Chirped-Pulse Millimeter-Wave Spectroscopy. The 260−295 GHz spectrometer has been described previously,[19] and only minor updates to the electronic setup will be described here. A schematic diagram of this spectrometer appears in Figure 3. The spectrometer employs the same single-frequency source scheme described above. The 9.375 GHz PDRO serves as the sampling clock for the AWG, and this signal is mixed with the two output channels of the AWG on the up- and downconversion arms of the spectrometer. After mixing with the PDRO, the chirped excitation pulse is filtered to remove the lower sideband and sent to a 24× active multiplication chain (Virginia Diodes AMC291). The molecular FID is downconverted in a subharmonic mixer, where the LO is generated by mixing the output of the second channel of the AWG with the PDRO, filtering to pass the upper sideband, and multiplying by a factor of 12 in the integrated detection module (Virginia Diodes MixAMC156). The downconverted signal passes through a DC block, before being amplified and digitized as in the W-band spectrometer. The 35 GHz of bandwidth was collected in three acquisitions with single sideband detection, and 1 million FIDs were averaged. The full spectrum of furan collected with this spectrometer appears in Figure 4.

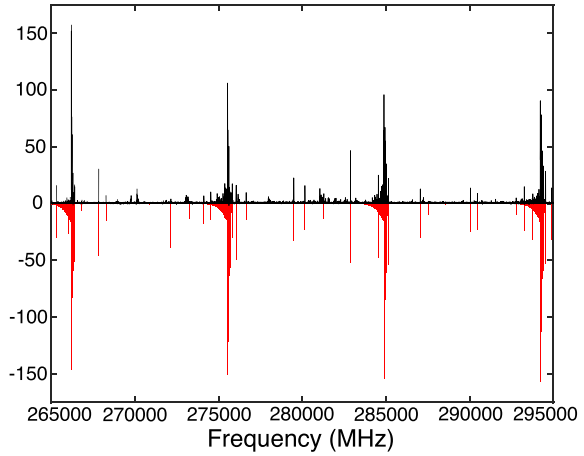

Figure 4. Room-temperature spectrum (black, top) of furan collected with the 260−295 GHz spectrometer and a simulated spectrum (red, bottom) using the constants from Table 1. The dominant spectral features, separated by approximately $(A + B)/2 \approx 9.3$ GHz, consist of a tight cluster of strong R lines, overlapping a weaker ladder of Q lines.

In this experiment, the sample cell is an 8 foot gold-plated WR42 waveguide cell with infrared (IR)-grade fused silica windows. Integration of a waveguide cell into a CP-FT spectrometer has been described previously at centimeter

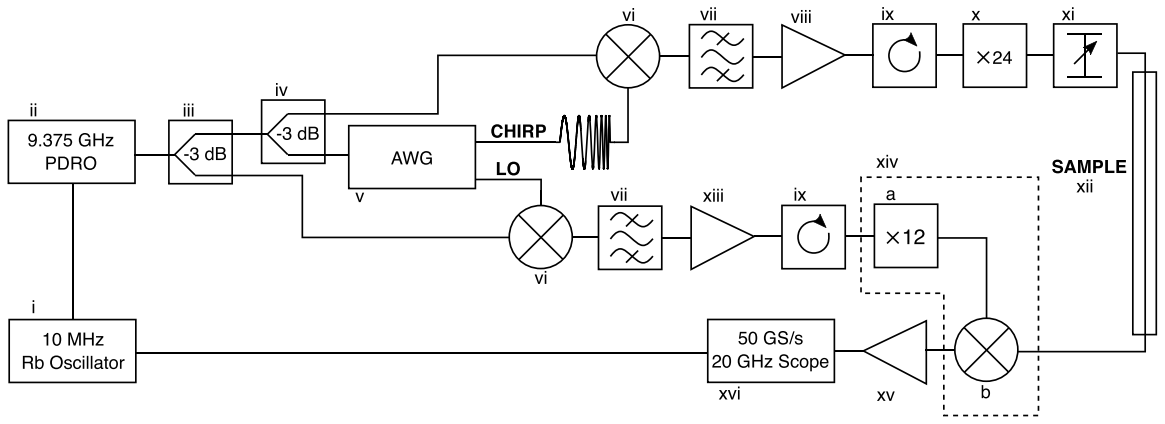

Figure 3. Schematic diagram of the high-frequency 260−295 GHz spectrometer. Similar to the W-band instrument, a 9.375 GHz PDRO serves as both the sampling clock for the AWG and as a fixed frequency source for upconversion of the chirped excitation pulse and the local oscillator signal. In both arms of this spectrometer, the upper sideband is selected by a bandpass filter (vii), amplified, and passed through an isolator. The excitation pulse is multiplied by a factor of 24 in the Virginia Diodes AMC291 module (x) before entering the waveguide cell (xii) containing the molecular sample. The molecular FID is directed into the subharmonic mixer (b) of the Virginia Diodes MixAMC156 module (xiv). This integrated module also provides active multiplication by a factor of 12 (a) for the LO signal from channel 2 of the AWG. The downconverted signal is amplified and digitized directly on a high-speed oscilloscope (xvi). A complete part list for this spectrometer may be found in the Supporting Information.

https://doi.org/10.1021/acsearthspacechem.1c00182
ACS Earth Space Chem. 2021, 5, 2986−2994

wavelengths.[20,21] We note that the use of a WR42 waveguide (10.668 × 4.318 mm interior dimensions) allows for the propagation of many TE modes in the 260−295 GHz range. Advantages of an overmoded design relative to a fundamental waveguide cell have been previously demonstrated[21] and include fewer wall collisions, reduced attenuation of the radiation, and improved cross-sectional overlap of the gas sample and electric field. Radiation is coupled into and out of the cell by a series of tapered transitions to the WR3.1 waveguide of the broadcast and detection units. The cell and sample fill line are evacuated by means of a small turbomolecular pump (Pfeiffer Balzers TPU 170). The sample pressure was monitored with a capacitance manometer pressure gauge (MKS Baratron 627D) and typically held around 10 mTorr to avoid strong pressure broadening of transitions. We observed typical line widths of ∼750 kHz at 275 GHz. The sample of furan was obtained from Millipore-Sigma (≥99% purity) and used without further purification in both spectroscopic experiments.

2.3. Quantum Chemical Calculations. Electronic structure calculations of furan were performed to assist in the assignment of low-lying vibrational excited states. Geometry optimizations and force field calculations were carried out using the CFOUR suite of programs,[22] employing second-order Møller−Plesset perturbation theory (MP2) coupled-cluster theory including perturbative triple excitations [CCSD(T)] under the frozen-core (fc) approximation as implemented in the xncc module, alongside the ANO0 basis set.[23] Calculations were performed on a Linux workstation, comprising 24 AMD 3960X threadripper cores and 64 GB of RAM, using the latest public release of CFOUR compiled with Intel Math Kernel Libraries (MKL) 2020 and OpenMP. To determine the anharmonic coupling and vibration−rotation interaction terms for vibrationally excited states, we performed second-order vibrational perturbation theory (VPT2) calculations,[24] computing the cubic force fields via finite differences of analytic second derivatives.

3. SPECTROSCOPIC ANALYSIS

3.1. Ground State. Furan is a planar, near oblate asymmetric top (κ = 0.9161) with a dipole moment of approximately 0.661 D[25] oriented along the inertial *a* axis and the C_{2v} symmetry axis (see Figure 5). The C_{2v} symmetry of furan produces a characteristic intensity alternation as a result of the nuclear spin statistics of the four hydrogen atoms. Rotational levels with K_a/K_c parity of ee and eo have a statistical weight of 10, while those with oe and oo parity have a statistical weight of 6. Using the PGOPHER spectral analysis software,[26] a *S*-reduced Watson rotational Hamiltonian in the III^r representation was fit to the experimental data for furan as well as the additional isotopologues and vibrational excited states discussed below. A minimum number of centrifugal distortion terms needed to fit the data within the experimental uncertainty were included. A total of 47 lines, corresponding to 33 unique frequencies in the W band, and 321 lines, corresponding to 178 unique frequencies in the 260−295 GHz region, were assigned and included in the fit. Lines were weighted as $1/\sigma^2$ according to the experimental accuracy of the two spectrometers: σ = 15 kHz for the W-band transitions and σ = 50 kHz for the high-frequency transitions. Blended lines were fit to the mean position weighted by the nuclear spin statistical weight of each line. Lines with a signal-to-noise ratio of less than 5 and partially resolved lines were deweighted in the fit by a factor of 2. In addition, we include two sets of previous observations: five high-resolution measurements of low-*J* transitions below 5 GHz[27] and 150 mmW rotational transitions between 130 and 260 GHz.[28] These observations were weighted according to their reported uncertainties: 25−50 Hz for the 5 GHz data from Tomasevich et al. and 50 kHz for the mmW data from Wlodarczak et al. An additional data set of 26 transitions observed in the K band by Stark modulation spectroscopy[25] was not included in the new fit because the residuals for these points were found to be much larger than the quoted 100 kHz uncertainty of the measurements; for completeness, these frequencies are included in the linelist, found in the Supporting Information, with a fit weight of zero.

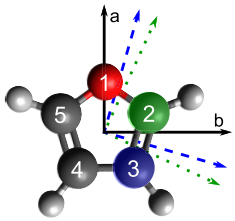

Figure 5. Inertial axis system and numbering scheme for the heavy atoms of furan. The *a* axis and direction of the dipole moment correspond with the C_{2v} axis of symmetry. The inertial axes for 2-^{13}C furan (green, dotted) and 3-^{13}C furan (blue, dashed) are rotated by 25° and 16°, respectively. This results in allowed *a*- and *b*-type rotational transitions for these species.

Relative to previous work on the ground state,[28] we have determined two additional sextic centrifugal distortion constants and improved the statistical uncertainty of all parameters in the rotational Hamiltonian. The improvement in the spectroscopic description of furan is evident from the root-mean-square (rms) errors shown in Table 1. Using the constants presented in refs 28 and 29, we calculated a rms residual of 69 and 45 kHz, respectively, using the same data set as in our fit. In both cases, the larger residual is predominantly due to errors of more than 100 kHz for over a dozen *Q*-type transitions at the highest frequencies probed in our data set. While the room temperature infrared study of ref 29 probed the high-*J* levels involved in these transitions, the ground state fit in that work is strongly influenced by the much higher resolution data of ref 28, which does not extend to these high-*J* values. In a quiescent molecular cloud like TMC-1, where line widths of just 400 kHz at 300 GHz are typical, errors of this magnitude make confident assignment of weak lines challenging and hinder advanced analysis techniques, like spectral line stacking. This points to the importance of extending the frequency coverage of high-resolution rotational spectroscopy to predict rest frequencies with the accuracy required for unambiguous interstellar detection. The improved molecular constants for these species will facilitate new astronomical searches in the mmW region, where peak intensities in the Boltzmann distribution occur at temperatures relevant to many interstellar sources.

3.2. Carbon-13 Isotopomers. Several lines belonging to the two ^{13}C isotopomers of furan in natural abundance were identified in the new data sets. As a result of symmetry, the two isotopomers 2-^{13}C furan and 3-^{13}C furan each have an abundance of ∼2% relative to the main isotopologue. The single ^{13}C substitution reduces the symmetry of these species

https://doi.org/10.1021/acsearthspacechem.1c00182
ACS Earth Space Chem. 2021, 5, 2986−2994

Table 1. Experimental and Theoretical [fc-CCSD(T)/ANO0] Molecular Constants for Furan, in MHz[a]

	fit	*ab initio*	ref 28	ref 29
A	9447.12422(14)	9295.18	9447.12360(32)	9447.122818(22)
B	9246.74472(14)	9064.67	9246.74437(31)	9246.742627(22)
C	4670.82631(14)	4586.87	4670.82458(40)	4670.824790(21)
D_J ($\times 10^3$)	3.33763(38)	3.190	3.33431(40)	3.332739(20)
D_{JK} ($\times 10^3$)	−5.26342(26)	−5.018	−5.26547(64)	−5.26388(33)
D_K ($\times 10^3$)	2.28150(39)	2.168	2.28375(81)	2.2837(36)
d_1 ($\times 10^6$)	−51.379(35)	−51.011	−51.91(23)	−52.425(17)
d_2 ($\times 10^6$)	43.10(12)	44.211	42.605(187)	43.17(33)
H_J ($\times 10^9$)	3.64(28)			
H_{JK} ($\times 10^9$	−6.099(95)		−6.11(24)	−5.210(14)
H_{KJ} ($\times 10^9$)	8.04(17)		6.14(71)	5.234(18)
H_K ($\times 10^9$)	−3.99(26)			
N[b]	522/366		517/361[c]	517/361[c]
rms	0.029		0.069	0.045
σ[d]	0.53		1.21	0.85

[a]Constants determined from two previous studies are included in this table to facilitate comparison. Numbers in parentheses are 1σ uncertainties in units of the last reported digit. [b]Number of lines in fit/number of unique frequencies. [c]In comparison to previous fits, the very high precision measurements of ref 27 were neglected because those errors dominated the reduced root-mean-square deviation, resulting in a less meaningful comparison. [d]Reduced root-mean-square deviation of fit, unitless.

Table 2. Molecular Constants for Two ^{13}C Furan Isotopomers from This Work and Ref 30, in MHz[a]

	2-^{13}C furan	2-^{13}C furan (ref 30)	3-^{13}C furan	3-^{13}C furan (ref 30)
A	9295.5801(75)	9295.41	9403.944(16)	9403.73
B	9178.3656(92)	9178.23	9043.784(17)	9043.68
C	4616.22293(39)	4616.25	4608.09842(35)	4608.15
D_J ($\times 10^3$)	3.2644(53)		3.2540(23)	
D_{JK} ($\times 10^3$)	−5.158(13)		−5.1357(58)	
D_K ($\times 10^3$)	2.2395(82)		2.2266(38)	
N[b]	86/24	86/24	110/32	110/32
rms	0.030	35.091	0.033	39.329
σ[c]	0.42	381.41	0.43	524.08

[a]Numbers in parentheses are 1σ uncertainties in units of the last reported digit. [b]Number of lines in fit/number of unique frequencies. [c]Reduced root-mean-square deviation of fit, unitless.

to C_s and rotates the inertial axes, allowing for both *a*- and *b*-type transitions. Substitution at the α position rotates the inertial axes approximately 25° (see Figure 5) and results in similar intensities for *a*- and *b*-type lines. This effect is reduced for substitution at the β position, and *a*-type lines are anticipated to be about 1 order of magnitude stronger than *b*-type lines. While individual *a*- and *b*-type lines were identified in the spectrum of 2-^{13}C furan, no individual *b*-type transitions could be assigned in the spectrum of 3-^{13}C furan. Blended *a*- and *b*-type lines identified in our spectra are assigned to both the contributing *a*- and *b*-type transitions with equal weight for the 2-^{13}C species, but these blends are weighted 10:1 for *a*/*b* for the 3-^{13}C species. The only previous study of these isotopomers was performed on enriched samples in the K band by Stark modulation spectroscopy.[30] However, like the previous measurements for the main isotopologue, we find that the residuals for this data set are larger than the reported experimental uncertainty, and we do not include these data in our final fit. The Stark modulation spectroscopy data for furan and its isotopologues were used in the determination of the experimental structure,[30] and thus, it may be valuable to revisit this analysis with new higher resolution measurements using pure samples. Molecular constants obtained from our fits and from the previously reported analysis for each isotopomer are summarized in Table 2. The new observations of ^{13}C isotopomers in this work has led to reduced uncertainty of the rotational constants for these species by more than 1 order of magnitude and the first determination of three quartic centrifugal distortion constants.

3.3. Vibrational Excited States. We have also identified rotational transitions of two low-lying vibrational excited states, $1\nu_{11}$ at 600 cm^{-1} and $1\nu_{14}$ at 603 cm^{-1}, out-of-plane ring deformations with a_2 and b_1 vibrational symmetry, respectively. In the jet-cooled spectrum, the intensity of these lines is approximately 4% that of the ground-state lines, which corresponds to a vibrational temperature of ∼250 K. However, we were unable to identify any lines belonging to the next highest energy vibrational state at 721 cm^{-1}, suggesting a non-thermal vibrational state distribution in the molecular beam, as observed in previous studies.[31] In addition to our quantum chemical calculations and a previous infrared study[29] of these vibrational states, our assignment was aided by a reversal in the pattern of intensity alternations as a result of nuclear spin statistical weights between ν_{11} with a_2 vibrational symmetry and ν_{14} with b_1 vibrational symmetry, as shown in Figure 2. In addition, quantum chemical calculations of the vibration−rotation constants using VPT2 were found to be in excellent agreement with the experiment (Table 3), with percentage errors on the order of a few percent.

https://doi.org/10.1021/acsearthspacechem.1c00182
ACS Earth Space Chem. 2021, 5, 2986−2994

Table 3. Experimental and Theoretical [fc-CCSD(T)/ANO0] Vibration−Rotation Interaction Constants for the Excited States, ν_{11} and ν_{14}, in MHz[a]

mode	axis	experiment	*ab initio*
ν_{11}	*A*	23.8643(11)	22.659
	B	19.2552(11)	19.374
	C	−2.06222(65)	−2.070
ν_{14}	*A*	24.6214(10)	24.473
	B	25.0421(12)	24.808
	C	−1.33675(57)	−1.359

[a]Numbers in parentheses are 1σ uncertainties in units of the last reported digit, after error propagation.

A high-resolution synchrotron-based IR study of both states was conducted by Tokaryk et al.[29] Because transitions to the ν_{11} level of a_2 vibrational symmetry are forbidden from the ground state of a_1 vibrational symmetry, the analysis was based on a study of the fundamental ν_{18} band and the $\nu_{18}-\nu_{11}$ hot band. These authors identified a second-order Coriolis interaction between ν_{11} and ν_{14} but found no evidence for the allowed first-order *c*-axis Coriolis interaction. We found inclusion of a second-order Coriolis interaction between ν_{11} and ν_{14} essential to fitting our observations to a level near the experimental uncertainty. This perturbation operator has the form

$$H_{cor} = G^{c}_{11,14}(J_aJ_b + J_bJ_a)$$

The constants from a simultaneous fit of the ν_{11} and ν_{14} rotational transitions appear in Table 4. The band origins of ν_{11} and ν_{14} are fixed to the values determined by Tokaryk et al.[29]

As pointed out previously,[29] because these two out-of-plane ring deformations involve nuclear motion in the direction of the *c* axis, the classical Coriolis force as a result of rotation about this axis is expected to be small. Indeed, we are unable to fit our data set to a first-order Coriolis interaction without inclusion of high-order corrections to the coupling constant. Interactions with distant levels of either a_1 or b_2 vibrational symmetry are responsible for the second-order Coriolis interaction, with the ν_8 level (a_1) at 870.45 cm^{-1} and the ν_{21} level (b_2) at 873 cm^{-1} both feasible possibilities. Without further observations, it is not possible to definitively identify the intermediate state or states involved in this second-order perturbation.

Using the constants from ref 29 (Table 4) to simulate the rotational spectrum, we find a rms residual with our data set of more than 300 kHz. This error is dominated by a handful of low-*J* ν_{11} transitions with residuals between 500 kHz and 1.5 MHz. These low-*J* levels are sampled in our jet-cooled spectrum but not in the room-temperature IR spectra of ref 29, explaining the poor agreement for this small subset of transitions. A complete description of the levels sampled in this work and previous reports appears in the Supporting Information. Although we fit two fewer distortion constants than in ref 29, our rms fit residual of 68 kHz indicates an improved description of this coupled $\nu_{11}-\nu_{14}$ dyad. The greatest differences appear in the molecular constants for the ν_{11} state, where, for example, the *A* rotational constant differs by more than 100 kHz between the two fits.

While our weighted fit residual of 0.98 indicates an acceptable fit, this fit error is significantly larger than those obtained in the ground-state fits. By including many high-order, non-physical distortion constants in the description of ν_{11}, we can obtain an improved fit (σ = 0.71). The same treatment of ν_{14} with high-order distortion constants does not similarly improve the quality of the fit nor does the inclusion of additional correction terms to the Coriolis interaction between ν_{11} and ν_{14}. This analysis leads us to speculate that an additional perturbation of ν_{11} may be operative. In particular, high-*J* levels of ν_{11} may interact with high-*J*, high-K_c levels from the ν_{10} level of a_2 vibrational symmetry at 721.5 cm^{-1}.[17] Because the fundamental band of this out-of-plane C−H bending mode is IR-inactive, its frequency has only been characterized through observations of combination bands, and no rotationally resolved data exists for this state. New rotationally resolved measurements of the ν_{10} vibrational state will be important in disentangling this possible multi-state interaction.

4. ASTRONOMICAL SEARCH

A motivating drive for this work is to facilitate astronomical searches for heterocyclic molecules, following the recent discovery of aromatic rings in TMC-1.[2,5,6] Using the best fit molecular constants for the ground state of furan obtained in this study, we performed a search toward TMC-1 using the

Table 4. Molecular Constants for Vibrational Excited States of Furan from This Work and the IR Study of Ref 29, in MHz[a]

	this work		ref 29	
	ν_{11}	ν_{14}	ν_{11}	ν_{14}
A	9423.2599(11)	9422.80286(99)	9423.3745(90)	9422.8057(13)
B	9227.4895(11)	9221.7026(12)	9227.4200(87)	9221.6997(13)
C	4672.88853(63)	4672.16306(55)	4672.8887(18)	4672.16656(69)
D_J (×10^3)	3.3384(90)	3.2966(44)	3.3466(12)	3.29755(28)
D_{JK} (×10^3)	−5.242(23)	−5.125(12)	−5.2326(33)	−5.11503(48)
D_K (×10^3)	2.261(15)	2.1844(77)	2.2408(29)	2.17317(54)
d_1 (×10^6)			−171.4(18)	−64.37(33)
d_2 (×10^6)			42.84(93)	47.43(36)
$G^{c}_{11,14}$	3.4499(68)		3.4576(13)	
N^b	61/38	85/49	61/38	85/49
rms	0.068		0.308	
σ^c	0.98		14.61	

[a]Numbers in parentheses are 1σ uncertainties in units of the last reported digit. [b]Number of lines in fit/number of unique frequencies. [c]Reduced root-mean-square deviation of fit, unitless.

https://doi.org/10.1021/acsearthspacechem.1c00182
ACS Earth Space Chem. 2021, 5, 2986−2994

second data release of the GOTHAM collaboration survey, the same data set used to detect the large aromatic molecules cyanonaphthalene[5] and indene.[6] Details of the source, observations, and data reduction methods can be found in ref 32. With our latest data, we were unable to find individual lines in the GOTHAM data set that could be ascribed to furan.

In lieu of a detection, we turned to applying Bayesian forward modeling with Markov chain Monte Carlo (MCMC) sampling to perform a best effort analysis on upper limits to the column density of this molecule in TMC-1. This procedure was used earlier to characterize molecules without individual observable transitions (indeed all of the aforementioned aromatic species), and for successful detections, the procedure can be visualized as a matched filter spectrum.[16,33] These methods are implemented in molsim,[34] wrapping the affine-invariant sampler emcee,[35] and uses ArviZ[36] for analysis and visualization. Here, we encode knowledge and intuition of the chemistry and physics of TMC-1 and furan through the choice of prior distributions: we used the posterior distributions of a chemically related five-membered ring, 1-cyanocyclopentadiene,[4] as informative priors for MCMC sampling, comprising four velocity components, where each is described by a source size, column density, and radial velocity, with a shared excitation temperature and line width parameter. We fix the source sizes to their mean values because these parameters were the largest sources of uncertainty in our previous analyses, particularly for molecules without individual observable transitions. Furthermore, we modify the column density priors to be consistent with the column density of the pure hydrocarbon cyclopentadiene, recently reported by Cernicharo et al.[37] Those authors reported a joint column density (i.e., the sum of four velocity components) of $(1.2 \pm 0.3) \times 10^{13}$ cm^{-2}. This choice is based on the intuition that cyclopentadiene is more chemically similar to furan than 1-cyanocyclopentadiene, given the number of heavy atoms and corresponding structure.

To summarize, the MCMC sampling comprises 10 free parameters: four column densities and radial velocities, and a single shared excitation temperature and line width. We derive an upper limit for the column density of $<1.0 \times 10^{12}$ cm^{-2}, representing the 95th percentile of the marginalized posteriors. This new value represents an order of magnitude lower constraint on the upper limit for furan in TMC-1 relative to previous searches.[14] We can compare this value to that of cyclopentadiene, assuming a beam filling factor of unity, which suggests that furan is at least 10 times less abundant than a pure hydrocarbon five-membered ring, further confirming the peculiar depletion of heterocycles in this molecular cloud. The apparent absence can be rationalized as a combination of inefficient formation, efficient destruction, and poor detectability, owing to a relatively small dipole moment.

The chemical routes for production and destruction of heterocycles in the ISM remain speculative, with ionizing radiation believed to play an important role in both formation[38] and destruction[39] pathways. A recent approach from our group to understand the chemistry of dark molecular clouds applied machine learning models to learn and predict the chemical abundances in TMC-1 without knowledge of explicit chemical pathways[40] by conditioning simple regressors to reproduce and predict chemical inventories. Here, we applied the same models to predict the abundance of furan. While predictions varied between the different regressors, the Gaussian process model estimates a mean column density on the order of $10^{12\pm4}$ cm^{-2}, consistent with our current upper limit. The large uncertainty associated with this value reflects the fact that no heterocycle has yet to be discovered, thereby highlighting a significant gap in chemical space spanned by an otherwise diverse inventory of TMC-1.

5. CONCLUSION

Using two broadband spectrometers covering the mmW region from 75.6 to 99.6 GHz and from 260 to 295 GHz, we have performed a new investigation of the rotational spectrum of the aromatic heterocycle furan. Our analysis adds more than 200 newly observed transitions to the existing data set, enabling the determination of all rotational and quartic centrifugal distortion constants as well as four sextic constants. This complete set of spectroscopic parameters will allow for calculation of precise rest frequencies for furan across the mmW region for future astronomical searches. In addition, our data set reveals new transitions of the two carbon-13 isotopomers, enabling an improved determination of the rotational constants and three centrifugal distortion constants for these species. We have identified rotational transitions belonging to the two lowest energy vibrational states, ν_{11} and ν_{14}, for the first time and obtain a satisfactory fit of this coupled dyad by inclusion of a second-order Coriolis interaction. The relatively large fit residual suggests that an additional unidentified perturbation may influence ν_{11}. Further investigation of the low-energy vibrational modes, especially the IR-inactive mode ν_{10}, may be important in explaining this perturbation. Finally, we searched for furan in the quiescent molecular cloud TMC-1 using the second data release from the GOTHAM collaboration and obtained an upper limit of 1.0×10^{12} cm^{-2}. A comparison of this column density to that of the recently detected five-membered ring, cyclopentadiene, explicitly confirms the depletion of heterocycles relative to hydrocarbon cycles in this source.

■ ASSOCIATED CONTENT

Supporting Information

The Supporting Information is available free of charge at https://pubs.acs.org/doi/10.1021/acsearthspacechem.1c00182.

Component lists for the W-band and high-frequency spectrometers and summary of the current and previous data sets discussed in this article (PDF)

Linelists for furan, 2-^{13}C furan, 3-^{13}C furan, and the vibrational excited states of furan, ν_{11} and ν_{14}, in a format compatible with the PGOPHER spectral analysis software, with file extensions needing to be changed to .lin for use (ZIP)

■ AUTHOR INFORMATION

Corresponding Authors

Timothy J. Barnum − *Department of Chemistry, Massachusetts Institute of Technology (MIT), Cambridge, Massachusetts 02139, United States;* orcid.org/0000-0002-9363-9844; Email: tbarnum@mit.edu

Brett A. McGuire − *Department of Chemistry, Massachusetts Institute of Technology (MIT), Cambridge, Massachusetts 02139, United States; National Radio Astronomy Observatory, Charlottesville, Virginia 22903, United States;* orcid.org/0000-0003-1254-4817; Email: brettmc@mit.edu

https://doi.org/10.1021/acsearthspacechem.1c00182
ACS Earth Space Chem. 2021, 5, 2986−2994

Author

Kin Long Kelvin Lee − *Department of Chemistry, Massachusetts Institute of Technology (MIT), Cambridge, Massachusetts 02139, United States;* orcid.org/0000-0002-1903-9242

Complete contact information is available at: https://pubs.acs.org/10.1021/acsearthspacechem.1c00182

Notes

The authors declare no competing financial interest.

■ ACKNOWLEDGMENTS

The authors thank Robert Field (MIT) and Brooks Pate (University of Virginia) for the loan of equipment. This work was supported in part by funding from MIT. The National Radio Astronomy Observatory is a facility of the National Science Foundation operated under cooperative agreement by Associated Universities, Inc.

■ REFERENCES

(1) McCarthy, M. C.; McGuire, B. A. Aromatics and cyclic molecules in molecular clouds: A new dimension of interstellar organic chemistry. *J. Phys. Chem. A* **2021**, *125*, 3231−3243.

(2) McGuire, B. A.; Burkhardt, A. M.; Kalenskii, S.; Shingledecker, C. N.; Remijan, A. J.; Herbst, E.; McCarthy, M. C. Detection of the aromatic molecule benzonitrile (*c*-C_6H_5CN) in the interstellar medium. *Science* **2018**, *359*, 202−205.

(3) McCarthy, M. C.; Lee, K. L. K.; Loomis, R. A.; Burkhardt, A. M.; Shingledecker, C. N.; Charnley, S. B.; Cordiner, M. A.; Herbst, E.; Kalenskii, S.; Willis, E. R.; Xue, C.; Remijan, A. J.; McGuire, B. A. Interstellar detection of the highly polar five-membered ring cyanocyclopentadiene. *Nature Astronomy* **2021**, *5*, 176−180.

(4) Lee, K. L. K.; Changala, P. B.; Loomis, R. A.; Burkhardt, A. M.; Xue, C.; Cordiner, M. A.; Charnley, S. B.; McCarthy, M. C.; McGuire, B. A. Interstellar detection of 2-cyanocyclopentadiene, C_5H_5CN, a second five-membered ring toward TMC-1. *Astrophys. J., Lett.* **2021**, *910*, L2.

(5) McGuire, B. A.; Loomis, R. A.; Burkhardt, A. M.; Lee, K. L. K.; Shingledecker, C. N.; Charnley, S. B.; Cooke, I. R.; Cordiner, M. A.; Herbst, E.; Kalenskii, S.; Siebert, M. A.; Willis, E. R.; Xue, C.; Remijan, A. J.; McCarthy, M. C. Detection of two interstellar polycyclic aromatic hydrocarbons via spectral matched filtering. *Science* **2021**, *371*, 1265−1269.

(6) Burkhardt, A. M.; Lee, K. L. K.; Changala, P. B.; Shingledecker, C. N.; Cooke, I. R.; Loomis, R. A.; Wei, H.; Charnley, S. B.; Herbst, E.; McCarthy, M. C.; McGuire, B. A. Discovery of the pure polycyclic aromatic hydrocarbon indene (*c*-C_9H_8) with GOTHAM observations of TMC-1. *Astrophys. J., Lett.* **2021**, *913*, L18.

(7) Burkhardt, A. M.; Loomis, R. A.; Shingledecker, C. N.; Lee, K. L. K.; Remijan, A. J.; McCarthy, M. C.; McGuire, B. A. Ubiquitous aromatic carbon chemistry at the earliest stages of star formation. *Nature Astronomy* **2021**, *5*, 181−187.

(8) Joule, J. A.; Mills, K. *Heterocyclic Chemistry*, 5th ed.; John Wiley & Sons: Hoboken, NJ, 2010.

(9) Komiya, M.; Shimoyama, A.; Harada, K. Examination of organic compounds from insoluble organic matter isolated from some Antarctic carbonaceous chondrites by heating experiments. *Geochim. Cosmochim. Acta* **1993**, *57*, 907−914.

(10) Martins, Z.; Botta, O.; Fogel, M. L.; Sephton, M. A.; Glavin, D. P.; Watson, J. S.; Dworkin, J. P.; Schwartz, A. W.; Ehrenfreund, P. Extraterrestrial nucleobases in the Murchison meteorite. *Earth Planet. Sci. Lett.* **2008**, *270*, 130−136.

(11) McGuire, B. A. 2018 census of interstellar, circumstellar, extragalactic, protoplanetary disk, and exoplanetary molecules. *Astrophysical Journal Supplement Series* **2018**, *239*, 17.

(12) Dezafra, R. L.; Thaddeus, P.; Kutner, M.; Scoville, N.; Solomon, P. M.; Weaver, H.; Williams, D. R. W. Search for interstellar furan and imidazole. *Astrophys. J.* **1971**, *10*, 1−3.

(13) Kutner, M. L.; Machnik, D. K.; Tucker, K. D.; Dickman, R. L. Search for interstellar pyrrole and furan. *Astrophys. J.* **1980**, *242*, 541−544.

(14) Dickens, J. E.; Irvine, W. M.; Nummelin, A.; Møllendal, H.; Saito, S.; Thorwirth, S.; Hjalmarson, Å.; Ohishi, M. Searches for new interstellar molecules, including a tentative detection of aziridine and a possible detection of propenal. *Spectrochim. Acta, Part A* **2001**, *57*, 643−660.

(15) Giuliano, B. M.; Bizzocchi, L.; Pietropolli Charmet, A.; Arenas, B. E.; Steber, A. L.; Schnell, M.; Caselli, P.; Harris, B. J.; Pate, B. H.; Guillemin, J.-C.; Belloche, A. Rotational spectroscopy of imidazole: Improved rest frequencies for astrophysical searches. *Astron. Astrophys.* **2019**, *628*, A53.

(16) Loomis, R. A.; Burkhardt, A. M.; Shingledecker, C. N.; Charnley, S. B.; Cordiner, M. A.; Herbst, E.; Kalenskii, S.; Lee, K. L. K.; Willis, E. R.; Xue, C.; Remijan, A. J.; McCarthy, M. C.; McGuire, B. A. An investigation of spectral line stacking techniques and application to the detection of $HC_{11}N$. *Nature Astronomy* **2021**, *5*, 188−196.

(17) Mellouki, A.; Liévin; Herman, H. The vibrational spectrum of pyrrole (C_4H_5N) and furan (C_4H_4O) in the gas phase. *Chem. Phys.* **2001**, *271*, 239−266.

(18) Park, G. B.; Steeves, A. H.; Kuyanov-Prozument, K.; Neill, J. L.; Field, R. W. Design and evaluation of a pulsed-jet chirped-pulse millimeter-wave spectrometer for the 70−102 GHz region. *J. Chem. Phys.* **2011**, *135*, 024202.

(19) Steber, A. L.; Harris, B. J.; Neill, J. L.; Pate, B. H. An arbitrary waveform generator based chirped pulse Fourier transform spectrometer operating from 260 to 295 GHz. *J. Mol. Spectrosc.* **2012**, *280*, 3−10.

(20) Reinhold, B.; Finneran, I. A.; Shipman, S. T. Room temperature chirped-pulse Fourier transform microwave spectroscopy of anisole. *J. Mol. Spectrosc.* **2011**, *270*, 89−97.

(21) Huang, Y.-T.; Hotopp, K. M.; Dian, B. C.; Chappell, W. J. Microwave chemical sensing at room temperature using an over-moded waveguide design. *IEEE Trans. Microwave Theory Tech.* **2012**, *60*, 2886−2893.

(22) Matthews, D. A.; Cheng, L.; Harding, M. E.; Lipparini, F.; Stopkowicz, S.; Jagau, T.-C.; Szalay, P. G.; Gauss, J.; Stanton, J. F. Coupled-cluster techniques for computational chemistry: The CFOUR program package. *J. Chem. Phys.* **2020**, *152*, 214108.

(23) Almlöf, J.; Taylor, P. R. General contraction of Gaussian basis sets. I. Atomic natural orbitals for first- and second-row atoms. *J. Chem. Phys.* **1987**, *86*, 4070−4077.

(24) Auer, A. A.; Gauss, J.; Stanton, J. F. Quantitative prediction of gas-phase ^{13}C nuclear magnetic shielding constants. *J. Chem. Phys.* **2003**, *118*, 10407−10417.

(25) Sirvetz, M. H. The microwave spectrum of furan. *J. Chem. Phys.* **1951**, *19*, 1609.

(26) Western, C. M. PGOPHER, a program for simulating rotational, vibrational and electronic spectra. *J. Quant. Spectrosc. Radiat. Transfer* **2017**, *186*, 221−242.

(27) Tomasevich, G. R.; Tucker, K. D.; Thaddeus, P. Hyperfine structure of furan. *J. Chem. Phys.* **1973**, *59*, 131.

(28) Wlodarczak, G.; Martinache, L.; Demaison, J.; Van Eijck, B. P. The millimeter-wave spectra of furan, pyrrole, and pyridine: Experimental and theoretical determination of the quartic centrifugal distortion constants. *J. Mol. Spectrosc.* **1988**, *127*, 200−208.

(29) Tokaryk, D. W.; Culligan, S. D.; Billinghurst, B. E.; van Wijngaarden, J. A. Synchrotron-based far-infrared spectroscopy of furan: Rotational analysis of the ν_{14}, ν_{11}, ν_{18} and ν_{19} vibrational levels. *J. Mol. Spectrosc.* **2011**, *270*, 56−60.

(30) Bak, B.; Christensen, D.; Dixon, W. B.; Hansen-Nygaard, L.; Andersen, J. R.; Schottländer, M. The complete structure of furan. *J. Mol. Spectrosc.* **1962**, *9*, 124−129.

(31) Sanz, M. E.; McCarthy, M. C.; Thaddeus, P. Vibrational excitation and relaxation of five polyatomic molecules in an electrical discharge. *J. Chem. Phys.* **2005**, *122*, 194319.
(32) McGuire, B. A.; Burkhardt, A. M.; Loomis, R. A.; Shingledecker, C. N.; Lee, K. L. K.; Charnley, S. B.; Cordiner, M. A.; Herbst, E.; Kalenskii, S.; Momjian, E.; Willis, E. R.; Xue, C.; Remijan, A. J.; McCarthy, M. C. Early Science from GOTHAM: Project Overview, Methods, and the Detection of Interstellar Propargyl Cyanide ($HCCCH_2CN$ in TMC-1. *Astrophys. J., Lett.* **2020**, *900*, L10.
(33) Loomis, R. A.; Shingledecker, C. N.; Langston, G.; McGuire, B. A.; Dollhopf, N. M.; Burkhardt, A. M.; Corby, J.; Booth, S. T.; Carroll, P. B.; Turner, B.; Remijan, A. J. Non-detection of $HC_{11}N$ towards TMC-1: Constraining the chemistry of large carbon-chain molecules. *Mon. Not. R. Astron. Soc.* **2016**, *463*, 4175−4183.
(34) Lee, K. L. K.; Loomis, R. A.; Xue, C.; El-Abd, S.; McGuire, B. A. *molsim*, 2021.
(35) Foreman-Mackey, D.; Hogg, D. W.; Lang, D.; Goodman, J. emcee: The MCMC Hammer. *Publ. Astron. Soc. Pac.* **2013**, *125*, 306−312.
(36) Kumar, R.; Carroll, C.; Hartikainen, A.; Martin, O. ArviZ a unified library for exploratory analysis of Bayesian models in Python. *Journal of Open Source Software* **2019**, *4*, 1143.
(37) Cernicharo, J.; Agúndez, M.; Cabezas, C.; Tercero, B.; Marcelino, N.; Pardo, J. R.; de Vicente, P. Pure hydrocarbon cycles in TMC-1: Discovery of ethynylcyclopropenylidene, cyclopentadiene, and indene. *Astron. Astrophys.* **2021**, *649*, L15.
(38) Materese, C. K.; Nuevo, M.; Sandford, S. A. N- and O-heterocycles produced from the irradiation of benzene and naphthalene in H_2O/NH_3-containing ices. *Astrophysical Journal* **2015**, *800*, 116.
(39) Peeters, Z.; Botta, O.; Charnley, S. B.; Kisiel, Z.; Kuan, Y.-J.; Ehrenfreund, P. Formation and photostability of N-heterocycles in space I. The effect of nitrogen on the photostability of small aromatic molecules. *Astron. Astrophys.* **2005**, *433*, 583−590.
(40) Lee, K. L. K.; Patterson, J.; Burkhardt, A. M.; Vankayalapati, V.; McCarthy, M. C.; McGuire, B. A. Machine learning of interstellar chemical inventories. *Astrophys. J., Lett.* **2021**, *917*, L6.

https://doi.org/10.1021/acsearthspacechem.1c00182
ACS Earth Space Chem. 2021, 5, 2986−2994